Materials Science in Semiconductor Processing 40 (2015) 832–839

Contents lists available at ScienceDirect

Materials Science in Semiconductor Processing

journal homepage: www.elsevier.com/locate/matsci

Bulk and surface modification of TiO_2 with sulfur and silver: Synergetic effects of dual surface modification in the enhancement of photocatalytic activity

L. Gomathi Devi *, R. Kavitha, B. Nagaraj

Department of Post Graduate Studies in Chemistry, Central College City Campus, Dr. Ambedkar Street, Bangalore University, Bangalore 560001, India

ARTICLE INFO

Article history:
Received 12 March 2015
Received in revised form
30 June 2015
Accepted 24 July 2015

Keywords:
Titanium dioxide
Sulfur doping
Silver deposition
Surface sulfation
Surface Plasmon Resonance effect

ABSTRACT

Sulfur ion (S^{6+}) was incorporated into the TiO_2 lattice ($Ti_{0.85}S_{0.15}O_2$) using sulfur powder as precursor. 0.05% of silver was deposited on the surface of $Ti_{0.85}S_{0.15}O_2$ by photoinduced deposition method. The photocatalytic reactivity of TiO_2, Ag–TiO_2, $Ti_{0.85}S_{0.15}O_2$ and Ag–$Ti_{0.85}S_{0.15}O_2$ photocatalysts were probed for the degradation of a model compound congo red (CR) dye under UV/solar light illumination. FTIR and XPS results suggested that the dopant sulfur ion (S^{6+}) was incorporated into the TiO_2 crystal lattice at Ti^{4+} lattice site and the sulfur ions on the surface were modified as SO_4^{2-} active sites serving as electron withdrawing group. TEM and XPS analysis of Ag–$Ti_{0.85}S_{0.15}O_2$ has confirmed the deposition of silver in the Ag^0 state. Ag–$Ti_{0.85}S_{0.15}O_2$ shows better photoactivty under solar light irradiation when compared to all the other photocatalysts. The enhanced photocatalytic activity of this catalyst is attributed to the synergetic effects of the incorporated dopant electronic energy level with the dual surface modifications of the type SO_4^{2-} active centers and Schottky junctions created by metallic Ag^0. Further the deposited Ag particles plays a dual role one as a sensitizer due to the Surface Plasmon Resonance (SPR) effect and also acts as an electron trapper under solar light illumination reducing the recombination of photogenerated charge carriers.

1. Introduction

TiO_2 photocatalysis has attracted considerable attention for applications to environmental issues owing to its cheapness, non-toxicity and structural stability with suitable flat band potential [1,2]. However the rapid recombination of photo-induced charge carriers and poor solar light absorption efficiency results in low quantum yield as determined by its band gap which limits the practical application of TiO_2[3]. In order to maximize the utilization of solar light, many researchers have devoted extensive research work in modifying both bulk and surface structure of TiO_2[4,5]. Noble metal deposition on the surface of non metal doped titania is one of the effective strategies attempted to enhance the photocatalytic process. Doping of non metal ions into the TiO_2 lattice has been regarded as one of the effective method for the modification of electronic band structure to extend the wavelength of absorption from UV to the visible region by efficient band gap narrowing. Further, the deposition of noble metal particles on the surface of TiO_2 can hinder the recombination of photogenerated charge carriers by vectorial transfer of photogenerated electrons to the deposited nano metal islands [6–15]. Ag deposition on TiO_2 surface has attracted considerable interest for its application in the fields like photocatalysis, energy conversion, antibacterial activity and pollutant degradation [16–20]. In addition metallic silver is exceptional compared to all the other noble metals due to its work function suitability which is much lower than that of other noble metals like gold and platinum and further advantage in using silver comes from its band edge positions which can be altered by varying the size of the deposits with the conduction band (CB) edge of TiO_2[21–25]. In continuation of our work with sulfur doped titania, focus is mainly on the combined synergistic effects of lattice doping by sulfur ions (S^{6+} ions) and surface Ag metal deposition on the TiO_2 photocatalyst is attempted [26]. The photocatalytic activity of the above silver deposited sulphur doped TiO_2 (Ag–$Ti_{0.85}S_{0.15}O_2$) was evaluated by taking a model compound such as congo red (CR) dye molecule under both UV and solar light irradiation.

2. Experimental section

2.1. Materials

Titanium (IV) chloride ($TiCl_4 \geq 99.9\%$) was obtained from Merck Chemicals limited. Sodium hydroxide (NaOH), sulphuric acid (H_2SO_4) and $AgNO_3$ were from Sisco-chemical industries, Bombay.

* Corresponding author.
E-mail address: gomatidevi_naik@yahoo.co.in (L. Gomathi Devi).

http://dx.doi.org/10.1016/j.mssp.2015.07.070
1369-8001/

All the reagents used were of analytical grade. Double distilled water was used throughout the experiment.

2.2. Catalyst preparation

2.2.1. Preparation of TiO_2 and sulphur doped TiO_2 ($Ti_{0.85}S_{0.15}O_2$)

TiO_2 was prepared by the sol–gel method through the hydrolysis of $TiCl_4$ as reported earlier [27]. The TiO_2 prepared from the above method was heat treated at 600 °C to obtain anatase phase. Under these conditions, the catalyst is found to be highly crystalline and further rise in temperature to 700 °C, phase transformation from anatase to rutile takes place. The 600 °C calcined anatase TiO_2 was used for the incorporation of sulfur into TiO_2 lattice. A stoichiometric volume of sulfur solution (0.1 ml of 0.00602 g of sulfur prepared in 100 ml benzene) was added to the calculated amount of TiO_2 (1 g) to get the desired dopant concentration of 0.15 at %. This mixture was grinded in a mortar and it was dried in an oven at 120 °C for 1 h. The process of grinding is repeated for five times and the powder is finally calcined at 200 °C for 5 h. The calcination temperature is kept at 200 °C since the boiling point of sulfur is 445 °C. $Ti_{0.85}S_{0.15}O_2$ powder appears pale brown in color [26]. With the increase in annealing temperature from 300 °C to 500 °C the brown color of the photocatalyst disappears indicating the complete removal of S ions from the titania lattice.

2.2.2. Method of surface Ag deposition on TiO_2 and $Ti_{0.85}S_{0.15}O_2$

Ag^0 (0.05%) was deposited on the surface of TiO_2 and $Ti_{0.85}S_{0.15}O_2$ by the process of photoreduction of $AgNO_3$ in the presence of oxalic acid [28]. An aqueous solution of $AgNO_3$ (1.24×10^{-4} M), oxalic acid (5×10^{-3} M) along with TiO_2 /$Ti_{0.85}S_{0.15}O_2$ (1 g) were suspended in 1 L of distilled water and was stirred vigorously under UV irradiation for 40–50 min. The pH of the suspension was adjusted to 6.8–7.0 by the addition of 0.1 N NaOH solution. After the irradiation the solution was then allowed to stand for 6 h. The color of the reaction mixture changed to dark brown under UV-light, indicating the reduction of Ag^+ to Ag^0 and confirming the deposition of Ag^0 on the photocatalyst surface. Finally the metalized photocatalyst particles were filtered, washed, dried and was heated at 120° C for 2 h. Ag–TiO_2 and Ag–$Ti_{0.85}S_{0.15}O_2$ at this stage appears dark brown in color. The absence of silver in the aliquot sample was checked by chloride precipitation method confirming the complete deposition of silver metal on the photocatalyst surface.

2.3. Characterization of the catalyst

The Powder X-Ray Diffraction (PXRD) patterns were recorded using Philips pw/1050/70/76 X-ray diffractometer. FT-IR spectra were obtained using NICOLET IMPACT 400 D FTIR spectrometer in the range of 400–4500 cm^{-1} using potassium bromide as the reference. The Diffused Reflectance Spectra (DRS) of the photocatalyst samples in the wavelength range of 190–800 nm were obtained by using a UV–vis (31031PC UV–vis–NIR Instrument) spectrophotometer with $BaSO_4$ as reference standard. Surface morphologies of various samples were analyzed by using JSM840 Scanning Electron Microscope (SEM) analysis. An electron microprobe is used in the EDX mode. The XPS measurements were carried out using AXIS ULTRA from AXIS 165, integrated with Kratos patented Magnetic immersion lens, charge neutralization system and spherical mirror analyzer. All the binding energies were calibrated to the C 1s peak at 284.8 eV of the surface adventitious carbon. Transmission electron microscope (TEM) images were recorded using Philips CM200 operated at 20–200 kV.

2.4. Photochemical reactor

Experiments were carried out at room temperature using a circular glass reactor whose surface area is 176.6 cm^2. 125 W medium pressure mercury vapor lamp is used as the UV light source. Photon flux was found to be 7.8 mW/cm^2 by ferrioxalate actinometry whose wavelength peaks around 370 nm. The irradiation was carried out by direct focusing the light into the reaction mixture in open air condition at a distance of 29 cm. The reaction mixture was continuously stirred. Solar light experiments were performed under sunlight directly between 11 am to 2 pm when the solar intensity fluctuations were minimal. The experiments were conducted in the months of April–May at Bangalore, India. The latitude and longitude corresponding to this place are 12.58 N and 77.38 E respectively. The average solar intensity was found to be 0.776 kW m^{-2} (using solar radiometer). The intensity of the solar light was concentrated by using a convex lens and the reaction mixture was exposed to this concentrated sunlight. The solar radiation as a function of wavelength was measured by photometer, which shows the maximum around 450–500 nm. To avoid the error arising due to the fluctuations in solar intensity all the experiments were conducted simultaneously. A typical experiment contains 20 mg/L of CR dye solution along with 400 mg/L of the photocatalyst. The reaction mixture was stirred vigorously using magnetic stirrer for the entire time span of the experiment. Prior to irradiation, the reaction mixture was stirred for 30 min to ensure the establishment of an adsorption/desorption equilibrium. 5 ml aliquots were collected from the reaction suspension at definite time intervals and this solution is centrifuged and filtered through 0.45 μm Millipore filter to remove the catalyst particles for the UV–vis spectrophotometric analysis. The residual CR concentration is measured in the wavelength range of 200–800 nm.

3. Results and discussions

3.1. PXRD studies

The PXRD pattern of TiO_2, Ag–TiO_2, $Ti_{0.85}S_{0.15}O_2$ and Ag–$Ti_{0.85}S_{0.15}O_2$ photocatalysts are shown in Fig.1. The peaks at 2θ values of 25° (1 0 1), 38° (1 1 2), 48° (2 0 0), 54° (1 0 5), 55° (2 1 1), 62° (2 0 4) and 68° (1 1 6) corresponds to the anatase phase in all the four samples. No typical diffraction peaks corresponding to the silver was observed in silver deposited samples (Ag–TiO_2 and Ag–$Ti_{0.85}S_{0.15}O_2$). This suggests an even distribution of Ag nanoparticles which is below the PXRD detection limits. Further, the deposited Ag was not oxidized to Ag_2O on the TiO_2 surface as confirmed by the absence of the peak at 2θ values of 34.22° [29]. The average crystallite size was estimated based on the line broadening of (1 0 1) peak at $2\theta=25.3$ by using the Debye–Scherrer's equation $d=k\lambda/\beta\cos\theta$ where θ is the wavelength of the Cu Kα source, β is the full width at half maximum (FWHM) of the (1 0 1) diffraction plane, K is a shape factor (0.94) and θ is the angle of diffraction (Table 1). The average crystallite size was found to be 27.57, 12.00, 31.17 and 21.79 nm for TiO_2, $Ti_{0.85}S_{0.15}O_2$, Ag–TiO_2 and Ag–$Ti_{0.85}S_{0.15}O_2$ respectively. It could be observed that incorporation of sulfur atoms inhibits the crystal growth of TiO_2 particles [26] whereas the crystallite size of silver deposited $Ti_{0.85}S_{0.15}O_2$ increases on metallization. This increase in crystallite size may be due to the presence of Ag nanoparticles on the titania surface. The ionic radius of Ti^{4+} ion (0.068 nm) is greater than that of S^{6+} ion (0.029 nm). Usually anionic sulfur doping is difficult to achieve due to the large differences in the ionic radius of S^{2-} (0.17 nm) ion compared to the O^{2-} ion (0.122 nm). Further the formation of Ti–S bond is much more favorable and easier since the bond strength of the Ti–S bond (148.0 kJ mol^{-1}) is less than the already existing

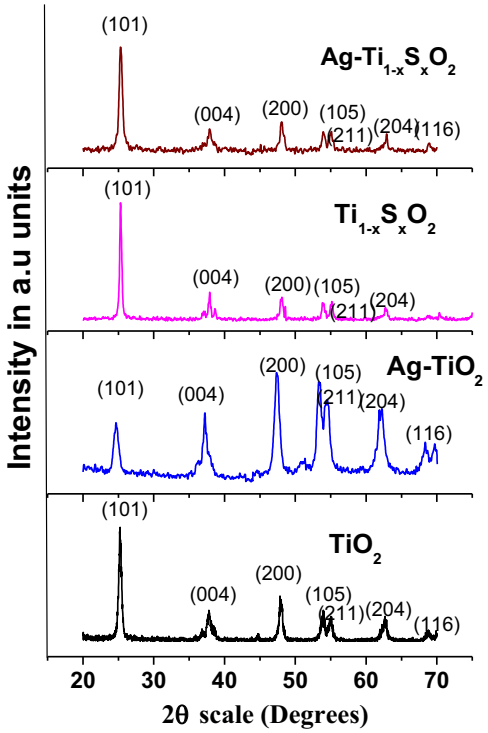

Fig.1. PXRD pattern of TiO_2, Ag–TiO_2, $Ti_{1-x}S_x$ O_2 and Ag–$Ti_{1-x}S_xO_2$ photocatalysts.

Table 1
Crystallite size, lattice parameters and cell volume as obtained by PXRD patterns for various photocatalysts.

Photocatalysts	Crystallite size (nm)	Lattice parameters (Å)	Cell volume $(Å)^3$
TiO_2	27.57	$a=b=$ 3.7828 $c=9.5023$	135.97
Ag–TiO_2	31.17	$a=b=3.8322$ $c=9.5585$	140.37
$Ti_{0.85}S_{0.15}O_2$	12.0	$a=$b$=3.7248$ $c=9.5028$	132.13
Ag–$Ti_{0.85}S_{0.15}O_2$	21.79	$a=b=3.7824$ $c=9.4386$	135.03

Ti–O bond (672.4 kJ mol^{-1}). Therefore substitution of S^{6+} ion at Ti^{4+} lattice sites is energetically, chemically and thermodynamically more favorable compared to substitution of S^{2-} ions at O^{2-} lattice sites by using sulfur powder as sulfur source [26]. Due to the size differences of Ti^{4+} and S^{6+} ions the crystallite size of sulfur doped $Ti_{0.85}S_{0.15}O_2$ sample decreases. However the crystallite size of Ag deposited samples can be analyzed in the following way: the silver nanoparticles are expected to mainly gather on the edges and corners of the TiO_2 grains [26b]. Since these positions are the highest energy domains and the deposition of Ag particles on these areas can lower the energy of the system to the largest extent [26b]. In such situations the crystallite size is not expected to increase. But however if the adsorption of Ag nanoparticles takes place preferably in the hollow sites between oxygen atoms in the TiO_2 lattice two types of binding mechanisms can be identified [26c]. In the stronger interaction the Ag orbitals overlaps with the surface oxygen atoms leading to charge transfer and ionic interactions. In the weaker interactions the highest occupied molecular orbital of Ag overlaps with the vacant unoccupied d-orbitals of the surface Ti atoms [26c]. In such a situation the crystallite sizes can increase with increase in Ag content up to certain optimum concentration [26c]. In general decrease or increase of the TiO_2 crystallite size depends on many factors like the method adopted for Ag metallization, experimental conditions, nature of reactants, and the concentration of silver and exact position of the deposition on the TiO_2 crystallite.

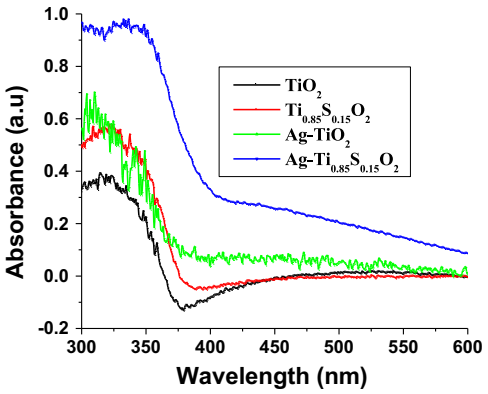

Fig. 2. UV–visible absorbance spectra of TiO_2, Ag–TiO_2, $Ti_{0.85}S_{0.15}O_2$ and Ag–$Ti_{0.85}S_{0.15}O_2$ photocatalysts.

3.2. DRS studies

The optical properties of all the catalysts were characterized by DRS studies (Fig. 2). The TiO_2 sample shows the band gap absorption onset at ~365 nm, corresponding to an intrinsic band gap of 3.21 eV. $Ti_{0.85}S_{0.15}O_2$ exhibits a slight increase in visible-light absorption in the wavelength range around ~365 to 436.61 nm owing to the incorporation of sulfur dopant into titania matrix resulting in the reduction of band gap to 2.54 eV. The presence of silver on TiO_2 and $Ti_{0.85}S_{0.15}O_2$ significantly influences the light absorption characteristics in the visible region. An increase in the extent of absorption in the visible region for these two catalysts above 400 nm can be measured by the area under the absorption curve, which is principally due to the Surface Plasmon Resonance (SPR) effect of Ag metal deposits [30]. The observed dramatic amplification of the visible-light absorption characteristics of Ag–$Ti_{0.85}S_{0.15}O_2$ can be attributed to the presence of sulfur dopant (response within 480 nm) and to the SPR effect of metallic Ag (response up to 600 nm).

3.3. FTIR analysis

FTIR spectra of TiO_2, Ag–TiO_2, $Ti_{0.85}S_{0.15}O_2$ and Ag–$Ti_{0.85}S_{0.15}O_2$ in the frequency range of 400–4000 cm^{-1} are as shown in the Fig. 3. The peaks observed at ~3400, 2930 and 2850 cm^{-1} are attributed to the Ti–OH bond [31]. The spectra shows relatively strong band at ~1630 cm^{-1} observed for all the photocatalysts which is due to the OH bending vibration of chemisorbed and/or physisorbed water molecule on the surface of the catalysts. The strong band in the range of 700–500 cm^{-1} is attributed to stretching vibrations of Ti–O–Ti bond [32]. $Ti_{0.85}S_{0.15}O_2$ and Ag–$Ti_{0.85}S_{0.15}O_2$ samples show peak at ~1046 cm^{-1} which corresponds to the vibrations of Ti–O–S bond confirming the incorporation of sulfur into TiO_2 lattice [33]. IR is one of the most prominent techniques which can be used to analyze the bonding nature of sulfate ion on the surface of TiO_2. The peak due to the asymmetric stretching frequency of the S=O bond appears at 1345 cm^{-1} which accounts for the +6 oxidation state of sulfur [33–35]. A band observed at ~1130 cm^{-1} corresponding to S–O stretching vibration can be assigned to the characteristic frequency

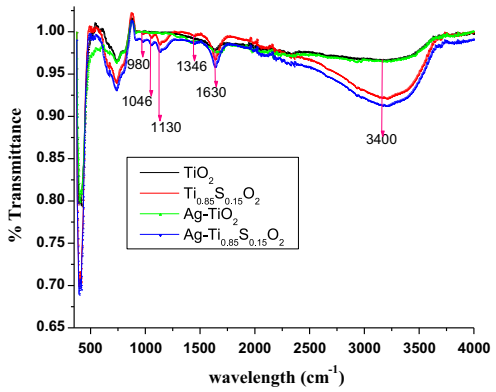

Fig. 3. FTIR spectra of TiO_2, Ag–TiO_2, $Ti_{0.85}S_{0.15}O_2$ and Ag–$Ti_{0.85}S_{0.15}O_2$ photocatalysts.

of either unidentate or bidentate SO_4^{2-} functional group which may be coordinated to either single Ti^{4+} ion (T_d) or two adjacent Ti^{4+} ions (C_{3v}) on the surface of TiO_2 lattice [34]. The IR characteristic peaks observed for the present photocatalyst sample at 1130, 1046 and 980 cm^{-1} confirms the presence of bidentate SO_4^{2-} corresponding to three S–O stretching bands. The sulfate ion having T_d symmetry is expected to show two infrared bands one assigned to ν_3 (1032–1044 cm^{-1} and 1117–1143 cm^{-1}) and the other for ν_4 (645–604 cm^{-1}) [35 b]. The ν_4 bands could not be monitored in the present case since TiO_2 bands (Ti–OH and Ti–O–Ti) overlap with the ν_4 vibrations of sulfate ion. Therefore ν_3 bands become more prominent to monitor the binding of SO_4^{2-} in this case [35b]. Bidendately co-ordinated sulfate groups have lower symmetry corresponding to C_{3v} exhibiting ν_1 (A_1) medium intensity band, ν_3 (A_1+E) and ν_4 (A_1+E) strong IR active bands which appears at 980 cm^{-1} (ν_1), 1046 cm^{-1} (ν_3) and 1130 cm^{-1}(ν_3) frequencies [35b]. The presence of these bands for $Ti_{0.85}S_{0.15}O_2$ and Ag–$Ti_{0.85}S_{0.15}O_2$ samples confirms the bidentate coordination of surface sulfate with lower C_{3v} symmetry.

3.4. SEM and EDX analysis

The surface morphologies and lattice compositions of TiO_2, Ag–TiO_2, $Ti_{0.85}S_{0.15}O_2$ and Ag–$Ti_{0.85}S_{0.15}O_2$ photocatalysts were studied using SEM (Fig. 4 A–D) and EDX analysis (Figure S1). There is significant difference in surface morphologies of the photocatalysts. The morphologies of TiO_2 (Fig. 4A) and Ag–TiO_2 particles exhibit flat plate like appearance (Fig. 4 B), sulfur doped TiO_2 ($Ti_{0.85}S_{0.15}O_2$ and Ag–$Ti_{0.85}S_{0.15}O_2$ as shown in Fig. 4 C and D) particles are spherical in shape. The Ag–$Ti_{0.85}S_{0.15}O_2$ particles appear to be highly spherical in shape in comparison to the other catalysts, which is due to the sulfur doping and also due to the low contact angle between the metallic Ag and the catalyst surface. A rough surface morphology was observed for TiO_2 with higher aggregation. The specific surface area of the bulk and surface modified catalyst is high compared to TiO_2. Further it can be observed that silver particles are highly dispersed on TiO_2 surface with intimate contact between them.

EDX analysis confirmed the presence of silver on Ag–TiO_2 and Ag–$Ti_{0.85}S_{0.15}O_2$ samples. The observed atom percentage of oxygen, titanium, sulfur and silver was found to be around 53.31, 46.33, 0.19 and 0.18% respectively for Ag–$Ti_{0.85}S_{0.15}O_2$ sample.

3.5. XPS analysis

The chemical state of various atoms in TiO_2 and Ag–$Ti_{0.85}S_{0.15}O_2$ was investigated by XPS analysis. Though the presence of silver was confirmed by EDX analysis, its presence on the surface of TiO_2 was confirmed by XPS analysis. The presence of Ti 2p, O1s, S 2p and Ag 3d in the photocatalyst samples were studied by measuring their binding energies by XPS technique as shown in Fig. 5. The binding energy peaks of Ti $2p_{3/2}$ and Ti $2p_{1/2}$ were found at 459.50 eV and 465.43 eV for undoped TiO_2 (Supplementary Figure S2a). These Ti 2p peaks were found at 459.71 eV and 465.43 eV for Ag–$Ti_{0.85}S_{0.15}O_2$ (Fig. 5a) [36 a]. The observed positive shift of 0.21 eV in the binding energy of Ti $2p_{3/2}$ for Ag–$Ti_{0.85}S_{0.15}O_2$ in comparison with TiO_2 can be ascribed to the sulfur incorporation into the TiO_2 lattice and this shift can also be caused by the presence of bidentate SO_4^{2-} structure on the adjacent

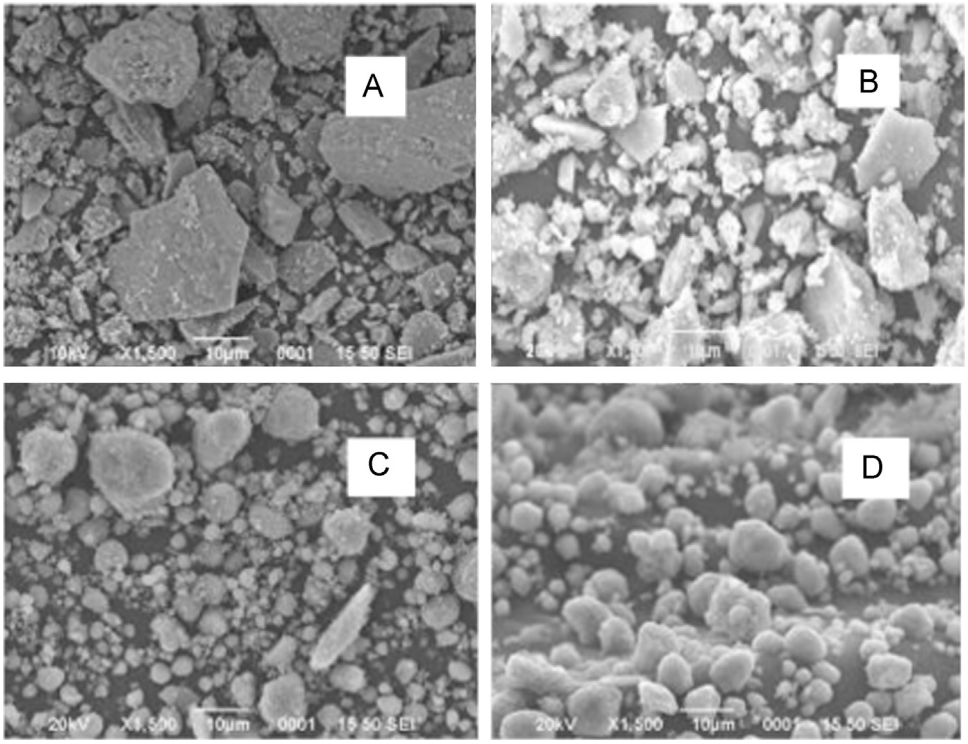

Fig. 4. SEM images of (A) TiO_2, (B) Ag–TiO_2 (C) $Ti_{1-x}S_xO_2$, and (D) Ag–$Ti_{0.85}S_{0.15}O_2$.

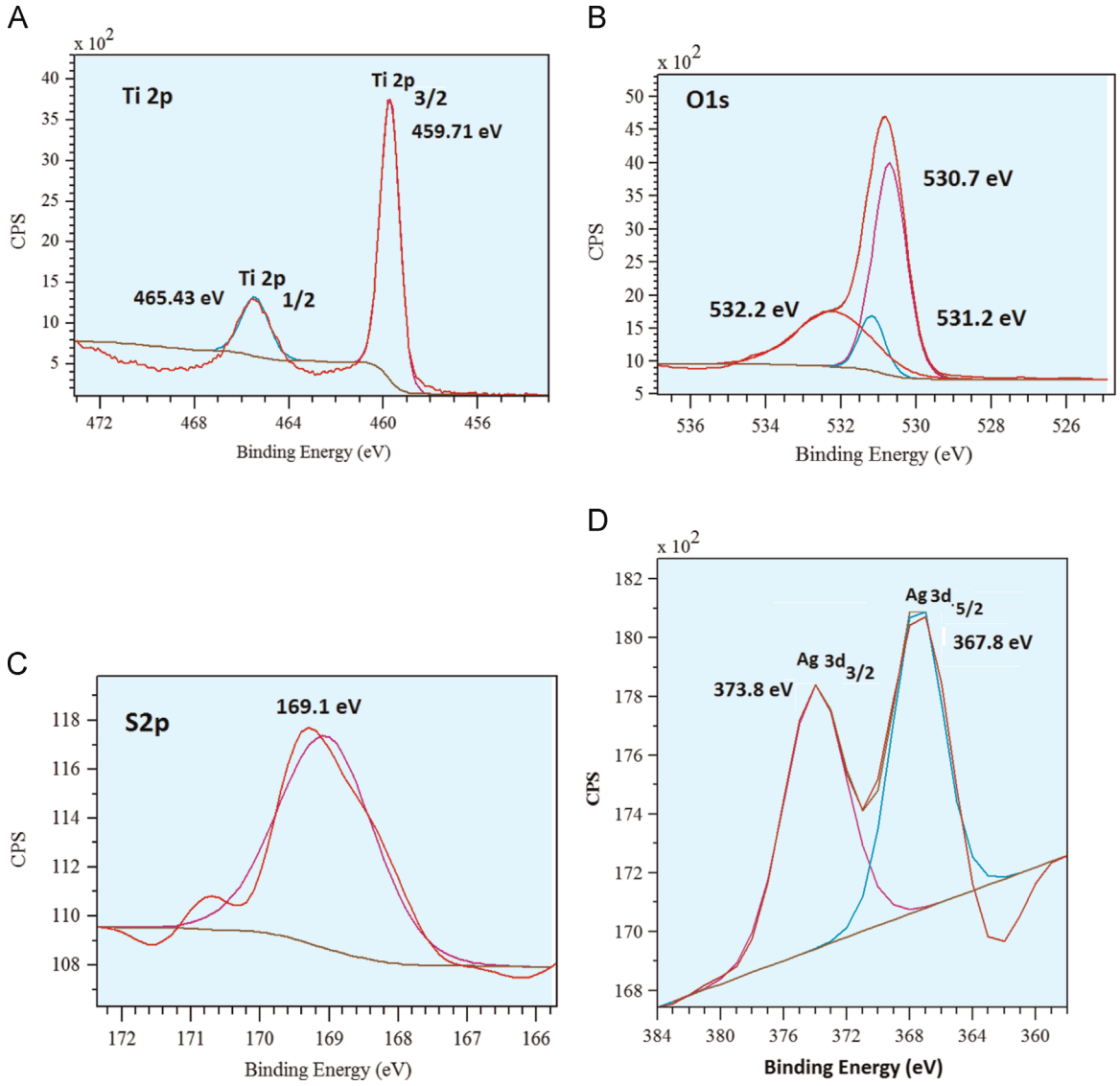

Fig. 5. High resolution XPS spectra of Ag–$Ti_{0.85}S_{0.15}O_2$ showing (a) Ti 2p, (b) O1s, (c) S2p, and (d) Ag 3d binding energy peaks.

Ti^{4+} ions [36b]. The XPS spectra of O1s peak for Ag–$Ti_{0.85}S_{0.15}O_2$ and TiO_2 revealed a well defined peaks at 530.4 and 530.7 eV for TiO_2 (Supplementary Figure S2b) and Ag–$Ti_{0.85}S_{0.15}O_2$ catalysts and a small shoulder peak centered at 532.20 eV which is observed only for Ag–$Ti_{0.85}S_{0.15}O_2$ (Fig. 5b). The peaks located at 530.7 and 531.2 eV can be accounted to the oxygen bonded with metal as Ti–O and the oxygen of surface-adsorbed water molecules as Ti–O–H [35]. The shoulder peak observed at 532.2 eV for Ag–$Ti_{0.85}S_{0.15}O_2$ sample can be assigned to the oxygen present in sulfate group [37]. The peak at 169.1 eV can be assigned to the +6 oxidation state of the sulfur. The presence of this peak indicates the confirmation of sulfur occupying the Ti^{4+} lattice site in the TiO_2 lattice (Fig. 5c) [38–40]. The deposition of silver on the surface of photocatalyst was confirmed by the presence of Ag 3d peaks in XPS spectra. The Ag 3d binding energy peaks corresponding to Ag $3d_{5/2}$ and Ag $3d_{3/2}$ appeared at 367.8 and 373.8 eV respectively (Fig. 5d). The spin orbital doublet splitting was found to be 6.0 eV which corresponds to silver as Ag^0 metallic state. The Ag incorporated in the TiO_2 lattice is expected to show binding energies values at 368.3 eV for $3d_{5/2}$ and 374.3 eV for $3d_{3/2}$. The absence of these peaks confirms the presence of silver only on the surface and not in the bulk lattice. The decrease in the binding energy values in the present case for Ag–$Ti_{0.85}S_{0.15}O_2$ can be attributed to the increase in the outer electron cloud density due to the transfer of the photo-induced electrons from the CB to the deposited Ag particles [41,42].

3.6. Transmission electron microscopy (TEM)

TEM image gives the distribution of the particles of TiO_2 and Ag–$Ti_{0.85}S_{0.15}O_2$ as shown in Fig. 6. The average particle size of the anatase TiO_2 nanocrystallites was found to be 34.26 nm. The Fig. 6A and B shows TEM images with two different magnifications for TiO_2. The average perimeter, thickness and length of the TiO_2 particles are found to be 26.78 nm, 3.54 nm and 9.86 nm respectively. The TEM micrograph of Ag–$Ti_{0.85}S_{0.15}O_2$ sample is shown in Fig. 6 C and D with two different magnifications. The average particle sizes of the Ag–$Ti_{0.85}S_{0.15}O_2$ were found to be 38.53 nm. The average perimeter, thickness and length of the Ag–$Ti_{0.85}S_{0.15}O_2$ are found to be 61.54 nm, 6.12 nm and 22.39 nm respectively. The average sizes of the deposited silver particles were found to be in the range of approximately 12–26 nm.

3.7. Photocatalytic activities of TiO_2, Ag–TiO_2, $Ti_{0.85}S_{0.15}O_2$ and Ag–$Ti_{0.85}S_{0.15}O_2$

The photocatalytic activities of the TiO_2, Ag–TiO_2, $Ti_{0.85}S_{0.15}O_2$ and

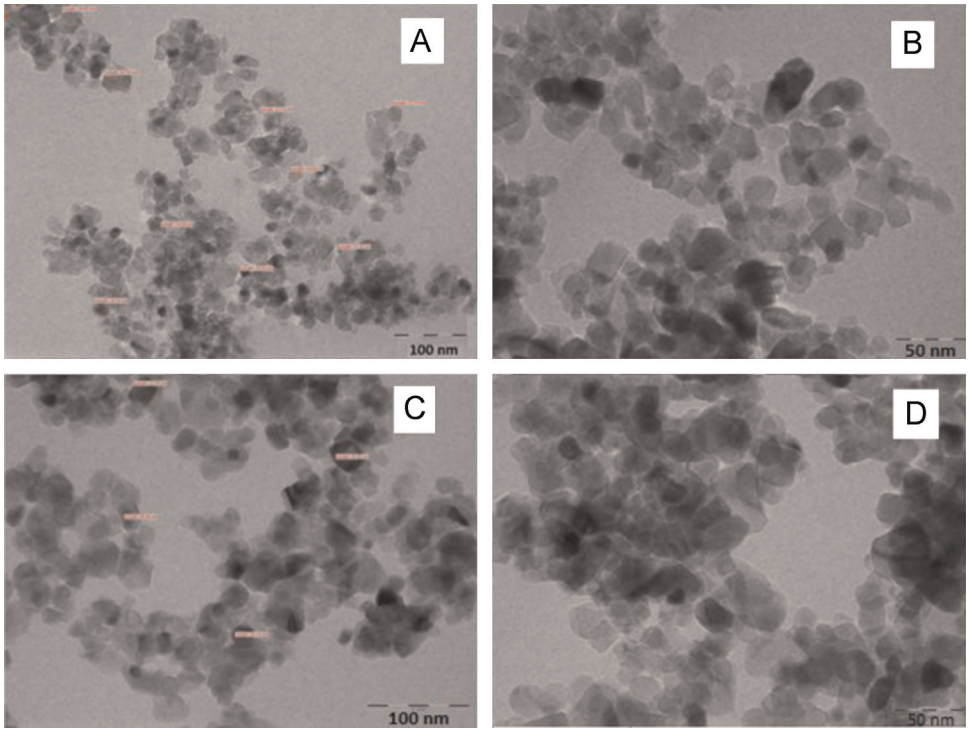

Fig. 6. TEM micrographs of TiO_2 particles (A) and (B) and Ag–$Ti_{0.85}S_{0.15}O_2$ particles (C) and (D) showing high and lower magnifications.

Ag–$Ti_{0.85}S_{0.15}O_2$ were evaluated for the degradation of CR dye under UV/solar light irradiation. A blank experiment containing only CR dye solution (in the absence of photocatalyst) under UV/solar illumination was performed in order to determine the contribution of direct photolysis. The experimental results confirmed the absence of degradation from direct photolysis. The photocatalytic activities of these catalysts under UV illumination show the following decreasing order: $Ti_{0.85}S_{0.15}O_2$ > Ag–$Ti_{0.85}S_{0.15}O_2$ > TiO_2 > Ag–TiO_2 (Fig. 7). However, under the solar light irradiation the order of activity was modified in the following way: Ag–$Ti_{0.85}S_{0.15}O_2$ > Ag–TiO_2 > $Ti_{0.85}S_{0.15}O_2$ > TiO_2. More precisely $Ti_{0.85}S_{0.15}O_2$ seems to be efficient catalyst under UV light whereas Ag–$Ti_{0.85}S_{0.15}O_2$ is most efficient under solar light irradiation. The activity of all the catalysts are found to be stable for three repeated uses and the degradation rates were concordant with the error bars of 0–2%.

The high activity of $Ti_{0.85}S_{0.15}O_2$ under UV illumination is attributed to the presence of sulfur dopant (S^{6+}) both in the TiO_2 bulk matrix and also on the surface where sulfur is present in the oxidized form as sulphate as confirmed by the IR studies (Table 2)

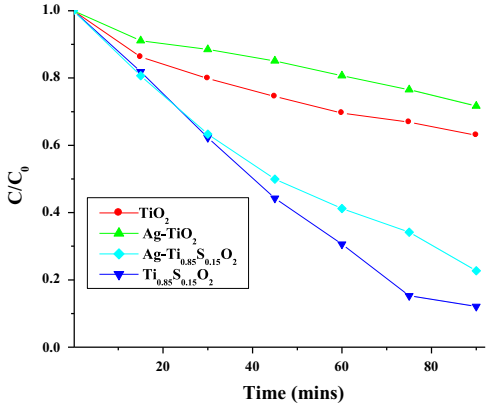

Fig. 7. Plot of C/C_0 versus time for the degradation of CR dye under UV light irradiation.

[26]. On UV illumination the electrons are excited from the valence band (VB) to the CB or to the S^{6+} dopant level which is located below the CB. These photoexcited electrons are transferred either from the impurity dopant level or from the CB to the surface modified sulfate groups and thereby suppressing the electron hole recombination rate [26]. The functional hydroxyl groups on TiO_2 surface acts as Bronsted acid sites and the Ti^{4+} ions coordinated to sulfate ion acts as Lewis acid sites. The high electronegativity of sulfur further enhances polarization of neighboring hydroxyl groups [43]. Interactions between SO_4^{2-} and Ti^{4+} are thought to be a driving force in the generation of a large amount of surface acidic sites on sulfated metal oxides [44]. Higher polarized states and higher surface acidity would favor the efficient trapping of photogenerated electrons in case of $Ti_{0.85}S_{0.15}O_2$. However, Ag deposited catalyst shows lesser efficiency than sulfur doped catalyst under UV illumination. In the case of Ag–TiO_2 and Ag–$Ti_{0.85}S_{0.15}O_2$ catalysts both semiconductor and the metal deposit absorb the photons. The photons absorbed by the semiconductor actively participate in the degradation reaction. The photons absorbed by the deposited metal are not available for the generation of charge carriers under UV light. In this case the metal could act as a shield for TiO_2 and these surface regions are not available for photon absorption thereby decreasing the efficiency [44b].

Ag–$Ti_{0.85}S_{0.15}O_2$ exhibits enhanced photocatalytic activity under solar light illumination compared to all the other

Table 2
Rate constant and percentage degradation values as obtained under UV and solar light irradiation for the degradation of CR dye.

Photocatalyst	UV light		Solar light	
	Rate constant $k \times 10^{-2}$ min^{-1}	Percentage degradation	Rate constant $k \times 10^{-2}$ min^{-1}	Percentage degradation
TiO_2	0.04844	40	0.239	4
Ag–TiO_2	0.03433	30	1.5160	75
$Ti_{0.85}S_{0.15}O_2$	0.24760	88	1.2440	67
Ag–$Ti_{0.85}S_{0.15}O_2$	0.15706	78	1.7260	80

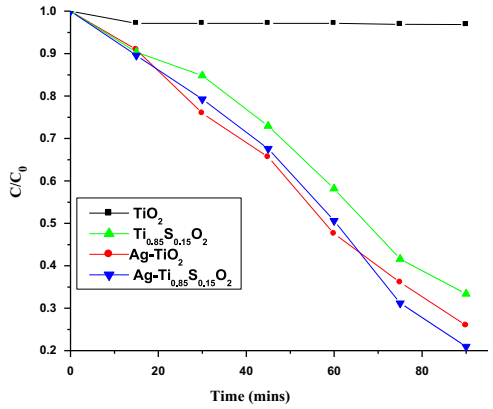

Fig. 8. Plot of C/C_0 versus time for the degradation of CR dye under solar light irradiation.

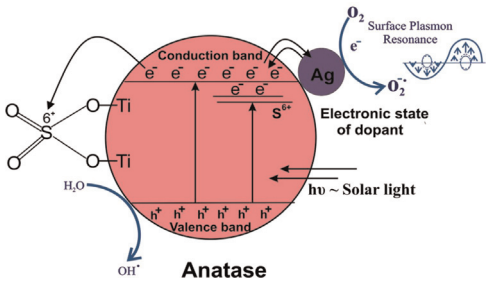

Fig. 9. Depiction of photogeneration of charge carriers in the bulk lattice and surface interfacial charge transfer mechanism in Ag–$Ti_{0.85}S_{0.15}O_2$ photocatalyst.

photocatalysts (Fig. 8), which can be attributed due to the synergistic effect observed between sulfur dopant, bidentately coordinated surface sulfate sites and deposited silver particles on the surface of TiO_2 (Fig. 9). The electrons are excited from VB to the S^{6+} dopant energy level (indirect band gap of TiO_2 ~2.84 eV) and these electrons can be trapped in three different ways: either by the surface modified SO_4^{2-} or by the metallic silver particles or by the surface adsorbed oxygen molecule [26]. This synergistic effect increases the life span of the photogenerated electron thereby reducing the electron hole recombination. The Schottky junction formed due to the contact of Ag metal with $Ti_{0.85}S_{0.15}O_2$ photocatalyst builds up an internal electric field close to the metal-semiconductor interface [45]. This induced internal electric field created inside or near the Schottky junction, forces the electrons and holes to move in different directions reducing their recombination rates [46]. Further, the electrons trapped by the metal deposits are detrapped efficiently to the adsorbed molecular oxygen on the surface to produce superoxide radicals. The photogenerated holes in the VB move to the surface of Ag–$Ti_{0.85}S_{0.15}O_2$ and reacts with surface adsorbed hydroxyl anion to produce highly reactive hydroxyl radical. The Fermi level of Ag (E=0.45 V vs SCE) is more positive than the CB of TiO_2[47], and hence the photogenerated electrons can be trapped by the Ag nanoparticles thereby lowering the Fermi level to more negative potentials [47]. Alternatively, under visible light Ag can also be excited by SPR effect and can inject electrons to the CB, working as an electron donor or as sensitizer under visible light. This mechanism is favorable only when the Ag metal deposit is of appropriate size. The position of Fermi level of Ag deposits varies with its sizes [48]. The Fermi level of the quantum sized Ag deposits lies above the CB hindering the electron transfer process and the Fermi levels of larger sized Ag deposits are pushed towards the VB and its position usually facilitates recombination. Hence appropriate size or amount of Ag is essential for efficient interfacial charge transfer mechanism. In the present case the optimum amount of silver was found to be 0.05%. The high specific surface area and spherical surface morphology of the modified catalyst plays a crucial role and they may possess more number of reactive sites enhancing the photocatalytic activity [7,26].

4. Conclusion

The enhanced photocatalytic activity of Ag–$Ti_{0.85}S_{0.15}O_2$ compared to $Ti_{0.85}S_{0.15}O_2$ under solar light irradiation can be attributed to the following synergetic effects: (i) the electronic energy levels created by the sulfur dopant enhances the visible light absorption (ii) the surface modification of sulfur as sulfate increases the surface acidic sites which can serve as trapping sites for the photogenerated electrons; (iii) the deposited silver serves both as electron sink and as sensitizer under visible light. Bulk modification of TiO_2 lattice by sulfur proved to be a better strategy to improve the activity under UV light. However both the bulk and surface modifications effectively decreased the rate of charge carrier recombination under visible light illumination. Therefore the photocatalytic activity of Ag–$Ti_{0.85}S_{0.15}O_2$ was found to be better under visible light.

Acknowledgements

The authors would like to acknowledge Department Science and Technology (DST-SERC, DST-IDP) and University Grants Commission (UGC), Government of India for the financial support.

Appendix A. Supplementary material

Supplementary data associated with this article can be found in the online version at http://dx.doi.org/10.1016/j.mssp.2015.07.070.

References

[1] (a) X. Chen, S.S. Mao, Chem. Rev 107 (2007) 2891–2959;
(b) J. Yu, W. Wang, B. Cheng, B.L. Su, J. Phys. Chem. C 113 (2009) 6743–6750;
(c) X.L. Hu, G.S. Li, J.C. Yu, Langmuir 26 (2010) 3031–3039;
(d) J.C. Yu, W. Ho, J. Yu, H. Yip, P.K. Wong, J. Zhao, Environ. Sci. Technol. 39 (2005) 1175–1179.
[2] (a) S.G. Kumar, L.G. Devi, J. Phys. Chem. A 115 (2011) 13211–13241;
(b) L.G. Devi, S.G. Kumar, Cent. Eur. J. Chem. 9 (2011) 959–961.
[3] G. Liu, L. Wang, H.G. Yang, H.M. Cheng, G.Q. Lu, J. Mater. Chem. 20 (2010) 831–843.
[4] L.G. Devi, R. Kavitha, Appl. Catal. B: Environ 140–141 (2013) 559–587.
[5] L.G. Devi, R. Kavitha, RSC Adv. 4 (2014) 28265–28299.
[6] (a) R. Kavitha, L.G. Devi, J. Environ. Chem. Eng. 2 (2014) 857–867;
(b) L.G. Devi, M.L. ArunaKumari, Appl. Surf. Sci. 276 (2013) 521–528.
[7] L.G. Devi, B. Nagaraj, K.E. Rajashekhar, Chem. Eng. J. 181–182 (2012) 259–266.
[8] B. Nagaraj, L.G. Devi, J. Mol, Catal. A: Chem. 390 (2014) 142–151.
[9] Y. Gao, P. Fang, F. Chen, Y. Liu, Z. Liu, D. Wang, Y. Dai, Appl. Surf. Sci. 265 (2013) 796–801.
[10] M. Wu, B. Yang, Y. Lv, Z. Fu, J. Xu, T. Guo, Y. Zhoa, Appl. Surf. Sci. 256 (2010) 7125–7130.
[11] (a) J. Yu, J. Xiong, B. Cheng, S. Liu, Appl. Catal. B: Environ. 60 (2005) 211–221;
(b) J. Yu, W. Wang, B. Cheng, B.L. Su, J. Phys. Chem. C 113 (2009) 6743–6750.
[12] (a) E. Kowalska, O.O.P. Mahaney, R. Abe, B. Ohtani, Phys. Chem. Chem. Phys. 12 (2010) 2344–2355;
(b) Y. Wu, H. Liu, J. Zhang, F. Chen, J. Phys. Chem. C. 113 (2009) 14689–14695.
[13] J. Yu, L. Qi, M. Jaroniec, J. Phys. Chem. C 114 (2010) 13118–13125.
[14] H. Tada, F. Suzuki, S. Ito, T. Akita, K. Tanaka, T. Kawahara, H. Kobayashi, J. Phys. Chem. B 106 (2002) 8714–8720.
[15] N. Hintsho, L. Petrik, A. Nechaev, S. Titinchi, P. Ndungu, Appl. Catal. B: Environ. 156–157 (2014) 273–283.
[16] Y. Wang, J. Yu, W. Xiao, Q. Li, J. Mater. Chem. A 2 (2014) 3847–3855.
[17] J. Yu, L. Yue, S. Liu, B. Huang, X. Zhang, J. Colloid Interface Sci. 334 (2009) 58–64.
[18] J. Yu, G. Dai, B. Huang, J. Phys. Chem. C 113 (2009) 16394–16401.

[19] R. Liu, P. Wang, X. Wang, H. Yu, J. Yu, J. Phys. Chem. C 116 (2012) 17721–17728.
[20] X. Zhou, G. Liu, J. Yu, W. Fan, J. Mater. Chem. 22 (2012) 21337–21354.
[21] P. Wang, B.B. Huang, X.Y. Qin, X.Y. Zhang, Y. Dai, J.Y. Wei, M.H. Whangbo, Angew. Chem. Int. Ed 47 (2008) 7931–7933.
[22] H.A. Atwater, A. Polman, Nat. Mater. 9 (2010) 205–213.
[23] (a) K. Nakayama, K. Tanabe, H.A. Atwater, Appl. Phys. Lett 93 (2008) 121904; (b) P.V. Kamat, J. Phys. Chem. Lett. 3 (2012) 663–672.
[24] D. Li, Z. Chen, Y. Chen, W. Li, H. Huang, Y. He, X. Fu, Environ. Sci. Technol. 42 (2008) 2130–2135.
[25] X. Li, Z. Zhuang, W. Li, H. Pan, Appl. Catal. A: Gen 429–430 (2012) 31–38.
[26] (a) L.G. Devi, R. Kavitha, Mater. Chem. Phys. 143 (2014) 1300–1308; (b) L. Ren, Y.P. Zeng, D. Jiang, Catal. Commun. 10 (2009) 645–649; (c) A.S. Mazheika, T. Bredow, V.E. Matulis, O.A. Ivashkevich, J. Phys. Chem. C 115 (2011) 17368–17377.
[27] L.G. Devi, G.M. Krishnaiah, J. Photochem. Photobiol. A Chem. 121 (1999) 141–145.
[28] E.S. Bardos, H. Czili, A. Horváth, J. Photochem. Photobiol. A: Chem. 154 (2003) 195–201.
[29] W. Zhou, H. Liu, J. Wang, D. Liu, G. Du, Jingjie Cui, ACS Appl. Mater. Interfaces 2 (2010) 2385–2392.
[30] P. Christopher, D.B. Ingram, S. Linic, J. Phys. Chem. C 114 (2010) 9173–9177.
[31] Y. Wang, Y. Huang, W. Ho, L. Zhang, Z. Zou, S. Lee, J. Hazard. Mater. 169 (2009) 77–87.
[32] E. Bae, W. Choi, Environ. Sci. Technol. 37 (2003) 147–152.
[33] S.T. Hussain, K. Khan, R. Hussain, J. Nat. Gas Chem. 18 (2009) 383–391.
[34] (a) D.I. Sayago, P. Serrano, O. Bohme, A. Goldoni, G. Paolucci, E. Roman, J. A. Martin-Gago, Surf. Sci 482–485 (2001) 9–14; (b) S.J. Hug, J. Colloid Interface Sci. 188 (1997) 415–422.
[35] (a) Z. Zhu, Z. Liu, H. Niu, S. Liu, T. Hu, T. Liu, Y. Xie, J. Catal. 197 (2001) 6–16; (b) K. Nakamoto, J. fujita, s Tanaka, M. Kobayashi, J. Am. Chem. Soc. 79 (1957) 4904–4908.
[36] (a) J.G. Li, R. Buchel, M. Isobe, T. Mori, T. Ishigaki, J. Phys. Chem. C 113 (2009) 8009–8015; (b) Y. Niu, M. Xing, B. Tian, J. Zhang, Appl. Catal. B: Environ 115–116 (2012) 253–260.
[37] A.Y. Kim, M. Kang, Int. J. Photoenergy (2012) 618642 , Article ID.
[38] J.C. Yu, W. Ho, J. Yu, H. Yip, P.K. Wong, J. Zhao, Environ. Sci. Technol. 39 (2005) 1175–1179.
[39] C.W. Dunnill, Z.A. Aiken, A. Kafizas, J. Pratten, M. Wilson, D.J. Morgan, I. P. Parkin, J. Mater. Chem. 19 (2009) 8747–8754.
[40] E. Roman, J.L.D. Segovia, J.A.M. Gago, G. Comtet, L. Hellner, Vacuum 48 (1997) 597–600.
[41] Y. Zheng, L. Zheng, Y. Zhan, X. Lin, Q. Zheng, K. Wei, Inorg. Chem. 46 (2007) 6980–6986.
[42] J. Li, J. Xu, W. Dai, K. Fan, J. Phys. Chem. C 113 (2009) 8343–8349.
[43] (a) X.Z. Fu, W.A. Zeltner, Q. Yang, M.A. Anderson, J. Catal. 168 (1997) 482–490; (b) X. Wang, J.C. Yu, Y. Hou, X. Fu, Adv. Mater. 17 (2005) 99–102.
[44] A. Nakajima, H. Obata, Y. Kameshima, K. Okada, Catal. Commun. 6 (2005) 716–720.
[45] A. Bumajdad, M. Madkour, Phys. Chem. Chem. Phys. 16 (2014) 7146–7158.
[46] A. Bumajdad, M. Madkour, Y.A. Moneam, M.E. Kemary, J. Mater. Sci. 49 (2014) 1743–1754.
[47] Z. Wang, J. Liu, W. Chen, Dalton Trans. 41 (2012) 4866–4870.
[48] A. Takai, P.V. Kamat, ACS Nano 5 (2011) 7369–7376.